Sensor Selection With Cost Function Using Nondominated-Solution-Based Multiobjective Greedy Method

Yuji Saito, Kumi Nakai, Takayuki Nagata, Keigo Yamada, Taku Nonomura, Kazuki Sakaki, and Yoshio Nunome

***Abstract*—In this study, a new greedy sensor selection algorithm with a cost constraint is proposed based on a nondominated-solution-based multiobjective greedy (NMG) method, and its performance is investigated by comparing it with a previously proposed method. The cost function is simultaneously considered with the D-optimality criterion, and the sensor set is selected based on the idea of the nondominated solution. Although a multiobjective optimization method for sensor selection with a cost constraint was previously considered based on the linear combination of the objectives, it requires a hyperparameter that determines the balance between the actual objective and the cost of the optimization. On the other hand, the proposed algorithm can obtain the Pareto solution without tuning the balance between the actual objective and the cost. We demonstrate the effectiveness of the proposed algorithm on the three different real datasets that are related to the sea surface temperature field, the flowfield around an airfoil, and the combustion field in a rocket chamber. A binary cost function is virtually imposed for each potential sensor location, and a sensor selection problem with a cost constraint is simulated. The results of the numerical experiments demonstrated that the NMG method could field a Pareto solution, and the objective values of almost all the sensor sets at a certain cost selected by the proposed method are superior to those selected by the previous method.**

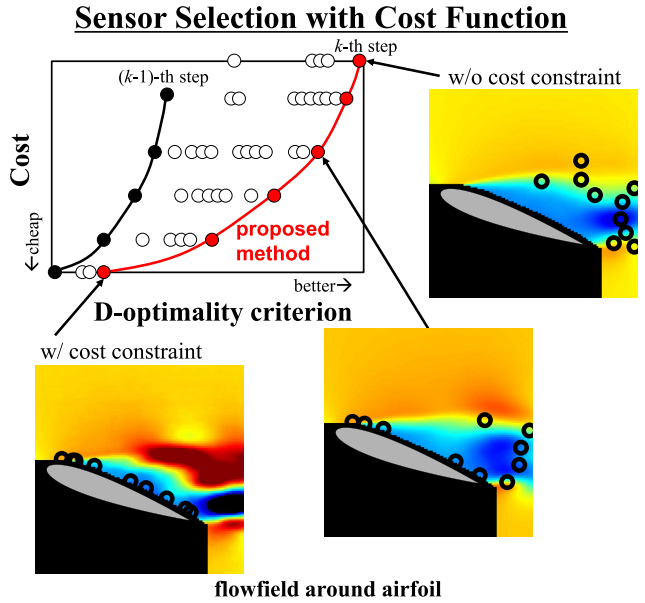

***Index Terms*—Cost constraint, data-driven sensor selection, greedy algorithm, multiobjective optimization.**

Manuscript received 20 May 2023; revised 3 July 2023, 28 August 2023, and 26 September 2023; accepted 14 October 2023. Date of publication 14 November 2023; date of current version 14 December 2023. This work was supported in part by Japan Science and Technology Agency (JST) ACT-X under Grant JPMJAX20AD; in part by JST Core Research for Evolutional Science and Technology (CREST) under Grant JPMJCR1763; in part by JST Fusion Oriented Research for disruptive Science and Technology (FOREST) under Grant JPMJFR202C; and in part by JST Moonshot Research and Development under Grant JPMJMS2287. The associate editor coordinating the review of this article and approving it for publication was Prof. Xiaofeng Yuan. *(Corresponding author: Yuji Saito.)*

Yuji Saito is with the Frontier Research Institute for Interdisciplinary Sciences, Tohoku University, Sendai, Miyagi 980-0845, Japan (e-mail: yuji.saito@tohoku.ac.jp).

Kumi Nakai is with the Department of Energy and Environment, National Institute of Advanced Industrial Science and Technology, Tsukuba, Ibaraki 305-8564, Japan (e-mail: kumi.nakai@aist.go.jp).

Takayuki Nagata, Keigo Yamada, and Taku Nonomura are with the Department of Aerospace Engineering, Tohoku University, Sendai, Miyagi 980-0845, Japan (e-mail: nagata@tohoku.ac.jp; keigo.yamada.t5@dc.tohoku.ac.jp; nonomuara@tohoku.ac.jp).

Kazuki Sakaki is with the Japan Aerospace Exploration Agency, Tsukuba 305-0047, Japan (e-mail: sakaki.kazuki@jaxa.jp).

Yoshio Nunome is with the Japan Aerospace Exploration Agency, Kakuda 981-1525, Japan (e-mail: nunome.yoshio@jaxa.jp).

Digital Object Identifier 10.1109/JSEN.2023.3328005

I. Introduction

A. Sensor Selection

OPTIMAL sensor selection with a cost constraint is relevant to several fields of scientific research and industry. For instance, in aerospace engineering applications, such as launch vehicles and satellites, optimal sensor selection is important for performance prediction, system control, fault diagnostics, and prognostics [1], [2]. This is because of the limitations of the measurement sensor installation and the high cost of the sensor device. Sensor optimization improves the quality and efficiency of measurements but often does not consider cost constraints. Alternatively, sensor selection methods that assume a uniform cost function have also been studied. A sensor selection problem without cost constraints is defined as an NP-hard combinatorial problem. For small-scale problems (selecting a small number of sensors from a small number of potential sensors), global optimization methods can provide an exact solution for the sensor selection problem. However, for large-scale problems (selecting sensors from a large number of potential sensors), the computational

cost is enormous. Several computational methods have been proposed for sensor selection, even in linear observation problems.

The quality of a set of sensors can be evaluated using the optimality criteria proposed in the optimal design of experiments [3]. These criteria are defined using the Fisher information matrix (FIM), which corresponds to the inverse of the error covariance matrix for estimation using sensors. Sensor optimization methods using typical design criteria, i.e., the D-, A-, and E-optimality criteria, have been proposed.

B. Related Works

Joshi and Boyd [4] formulated a sensor optimization problem using the D-optimality criterion. They relaxed the problem to a convex function and optimized the sensor location using semidefinite programming. The convex relaxation method could thereafter produce a globally optimal solution for the relaxed problem. The computational complexity is $\mathcal{O}(n^3)$, where n denotes the number of sensor candidates. For data used in fluid and combustion dynamics (e.g., high-speed cameras and numerical simulations), the number of candidate sensors is extremely large on a large scale. Therefore, further improvements in conventional sensor optimization methods are required. This algorithm was recently improved through the development of a randomized algorithm for acceleration [5]. Several convex optimization methods based on the proximal splitting algorithm have been proposed, including the alternating direction method of multipliers [6], [7], [8], [9]. Although a sensor selection method based on the proximal splitting algorithm that significantly reduces ($\mathcal{O}(n)$), the computational cost has been proposed [10], [11], and the computational cost is still high when applied to a problem with several degrees of freedom. Alternatively, a sensor selection method based on greedy algorithms that are faster than convex relaxation methods has been proposed [12], [13], [14], [15].

Manohar et al. [12] applied and extended the QR-based discrete empirical interpolation method, which is a greedy method, to sensor selection problems. Saito et al. [13] showed mathematically that the method proposed by Manohar et al. [12] is equivalent to the D-optimality-based greedy (DG) method when the number of sensors is less than that of the latent variables (i.e., undersampling). They also proposed a greedy method based on D-optimality that is efficient regardless of the number of sensors (i.e., oversampling). These greedy methods can find a solution that is within $(1-1/e)$ of the optimal solution when the objective function is monotone submodular and outperform the convex relaxation methods when the size of the problem increases [16], [17], [18]. Due to their fast calculations and reasonable performance, such greedy methods are more appealing for sensor selection. They have been extended for various purposes [19], [20], [21], [22], [23], [24], [25], [26], [27], [28], [29] and have been implemented in several applications [30], [31], [32], [33], [34], [35], [36], [37], [38], [39], [40], [41], [42].

Cost constraints are an important issue, as sensor placement is expensive and/or sensors often cannot be placed in the desired locations due to sensor placement costs. Furthermore, due to communication and energy constraints, wireless sensor networks must use a limited number of sensors [43], [44], [45]. Because radars have limited resources, the use of a limited number of sensors is critical in radar sensor networks [46], [47], [48], [49]. Clark et al. [19] proposed a QR-based greedy algorithm with a cost constraint for sparse sensor selection and demonstrated the effectiveness of this method on three different datasets with unique cost functions: eigenfaces, weekly sea surface temperature data, and vortex shedding of a fluid flowing around a cylinder. The previously proposed DG method with cost constraints does not perform multiobjective optimization, which maximizes the determinant and minimizes the cost; however, it can efficiently obtain the Pareto solution between the determinant and the cost. This method is also empirical in its formulation and adjusts the weights of the terms for which the costs are considered using a fixed parameter γ. Therefore, the previously proposed DG method for the cost constraints can be further improved by applying the general idea of multiobjective optimization to the determinant and cost. In addition, a previously proposed DG method with a cost constraint in the undersampling case was proposed; however, it has not yet been extended to the oversampling case. Nevertheless, oversampling is important, particularly when considering the sensor selection problem with a small number of latent variables. Yu et al. [50] considered the cost constraint problem for high-dimensional data with a view toward health research applications such as for diabetes. They efficiently solved the cost constraint problem using a projected gradient descent method and dynamic programming for the 0–1 knapsack problem; however, their convergence calculations are time-consuming. Therefore, this study focuses only on the greedy method, which is computationally fast.

The multiobjective genetic algorithm (MOGA) is a powerful method for solving multiobjective optimization problems (MOPs). Several MOGAs have been developed [51], [52], [53], and their application has been intensively studied in the engineering field, for instance, the optimization of the airfoil for aircraft and turbines [54], [55], [56], [57]. MOPs typically have a set of tradeoff solutions instead of an optimal solution. Thus, algorithms for solving MOPs typically produce nondominated solutions (Pareto-optimal solutions) that belong to the same rank (the Pareto-optimal front) and are deemed equally important, using the notion of Pareto dominance.

A previous study inspired by the MOGA proposed a nondominated-solution-based multiobjective greedy (NMG) method for sensor selection [26]. The previously proposed NMG method iteratively adds a new sensor to the set of sensors obtained in the previous step by simultaneously evaluating MOPs. The NMG method reserves sets of sensors corresponding to the nondominated solutions in a multiobjective-function space at each step of sensor selection. A previous study evaluated the selected sensor set by comparing the performance of the NMG method with those of various pure- and group-greedy [58] methods and showed that the NMG method outperformed the pure-greedy methods for all optimality measures. The extracted sensor subsets were compared with those of the NMG method, which is the best measure for each optimality criterion. Thus, the previously proposed

NMG method can be improved by multiobjective optimization over the DG method with cost constraints when applied to a selection problem with cost constraints. The aim of D-optimality for the optimal design of experiments is to improve and compare the previously proposed sensor selection method with a cost constraint [19]. Other methods, such as particle swarm optimization [59] and ant colony optimization [60], require careful adjustment of the hyperparameters to achieve optimal solutions, and their performance is not guaranteed. In contrast, the NMG method requires the adjustment of only a single hyperparameter $L_{\max}$, and the solution is improved by increasing this hyperparameter instead of the increase in the computational cost. Furthermore, a previous study provided theoretical evidence that the NMG method exhibits a performance guarantee when applied with monotone submodular functions, similar to a pure greedy method [26].

C. Contributions of This Study

The main contributions of this study are summarized as follows.

1) A new greedy sensor selection algorithm with a cost constraint is proposed based on the NMG method, and its performance is investigated by comparing it with a previously proposed method.
2) The NMG method simultaneously considers D-optimality for the optimal design of experiments and the cost constraint and applies the idea of Pareto ranking to select the sensor set.
3) The effectiveness of this algorithm on datasets related to the sea surface temperature field, the velocity field around an airfoil, and the temperature field in a rocket chamber is demonstrated.

II. Problem and Algorithm

This section introduces the sensor selection problem without cost constraints. Because the D-optimality criterion is considered in this study, a DG algorithm without cost constraints is explained. Next, the previously proposed DG algorithm with cost constraints is introduced. Finally, an NMG method for sensor selection with cost constraints is proposed.

A. D-Optimality-Based Greedy Without Cost Constraint

We define the sensor selection problem as follows:

$$\mathbf{y} = \mathbf{H}\mathbf{U}\mathbf{z} = \mathbf{C}\mathbf{z} \tag{1}$$

where $\mathbf{y} \in \mathbb{R}^p$ denotes the observation vector, $\mathbf{H} \in \mathbb{R}^{p\times n}$ denotes the sensor location matrix, $\mathbf{U} \in \mathbb{R}^{n\times r}$ denotes the sensor candidate matrix, $\mathbf{z} \in \mathbb{R}^r$ denotes the latent variable vector, and $\mathbf{C} \in \mathbb{R}^{p\times r}$ denotes the measurement matrix ($\mathbf{C} = \mathbf{H}\mathbf{U}$). Here, p, n, and r denote the number of sensors to be selected, the total number of sensor candidates, and the number of latent variables, respectively. The sensor location matrix $\mathbf{H}$ contains in each row an entry of unity indicating the determined sensor locations with zeros for remainders. Optimization without the cost constraint corresponds to the minimization of the volume of an ellipsoid, which represents the expected estimation error variance

$$\text{minimize}\, \det\left(\mathrm{E}\left[(\mathbf{z}-\tilde{\mathbf{z}})(\mathbf{z}-\tilde{\mathbf{z}})^\top\right]\right) \tag{2}$$

where operator $\mathrm{E}[\circ]$ denotes the expected value of the argument.

As described in [15], the objective function for sensor selection problems can be defined using the FIM based on the optimal design of experiments. Here, the D-optimality criterion is considered. The Cramér–Rao bound is inversely proportional to the FIM; this implies that it approaches a theoretically lower limit on the variance of any unbiased estimator for the parameter. The objective function based on the D-optimality criterion is expressed as follows:

$$f_{\mathrm{D}} = \begin{cases} \det\left(\mathbf{C}\mathbf{C}^{\mathsf{T}}\right), & p \le r \\ \det\left(\mathbf{C}^{\mathsf{T}}\mathbf{C}\right), & p > r. \end{cases} \tag{3}$$

Each sensor is selected by repeatedly selecting the best locations in terms of the maximization of f_{D} in each single-sensor subproblem. Simplified formulations are employed using the greedy method, as discussed in previous studies [13], [15]. The DG without the cost constraint is defined as "DG method without cost" and "DG w/o cost" in this article.

B. D-Optimality-Based Greedy Method With Cost Constraint

The general sensor placement problem with cost constraints is expressed as follows:

$$\text{minimize}\, \det\left(\mathrm{E}\left[(\mathbf{z}-\tilde{\mathbf{z}})(\mathbf{z}-\tilde{\mathbf{z}})^\top\right]\right) \quad \text{s.t.} \sum_{i=1}^{p} c_i \le B \tag{4}$$

where $\boldsymbol{c}$ and B denote the cost vector and the budget, respectively. The cost constraint is expressed as follows:

$$f_{\mathrm{C}} = \sum_{i=1}^{p} c_i \le B. \tag{5}$$

Clark et al. [19] derived a greedy algorithm for a relaxed version of the cost-constrained sensor placement problem, as expressed in (4), and a QR-based greedy algorithm based on the D-optimality criterion with a cost constraint. Therefore, the objective function for the sensor selection problem was defined using the D-optimality criterion of the FIM based on the optimal design of experiments, as explained in [15]. In the stepwise selection of the greedy method, only the kth sensor is selected in the kth step under the condition that the sensors up to $(k-1)$th are already determined. The optimization is expressed for each step (sensor selection) as follows:

$$\text{maximize}\, ||\mathbf{w}_i||^2 - \gamma c_i \tag{6}$$

where $\mathbf{w}_k = \mathbf{u}_{i_k}\mathbf{P}_{k-1}\mathbf{u}_{i_k}^\top$ ($\mathbf{P}$ denotes the projection matrix onto the row vector space of $\mathbf{C}$) and γ is a hyperparameter that determines the weight of the cost constraint. A previous study extended the QR-based greedy algorithm to cost constraints; however, the QR method without cost constraints maximizes the increment of the determinant (see [13]). Therefore, the extension of the QR method to cost constraints is a two-objective optimization of both the increment of the determinant and the cost. The two-objective optimization for

the D-optimality criterion and the cost from their formulation can be expressed as follows:

$$\begin{cases} \text{maximize} \ \dfrac{\det\left(\mathbf{C}_k\mathbf{C}_k^\top\right)}{\det\left(\mathbf{C}_{k-1}\mathbf{C}_{k-1}^\top\right)} - \gamma\displaystyle\sum_{i=1}^{k} c_i, & p \le r \\ \text{maximize} \ \dfrac{\det\left(\mathbf{C}_k^\top\mathbf{C}_k\right)}{\det\left(\mathbf{C}_{k-1}^\top\mathbf{C}_{k-1}\right)} - \gamma\displaystyle\sum_{i=1}^{k} c_i, & p > r. \end{cases} \tag{7}$$

In this study, based on the formulation of previous studies, we treat the two-objective optimization method of the D-optimality criterion and the cost function as "DG method with cost" or "DG w/ cost." In this study, the DG method with a cost constraint for undersampling is extended to oversampling. We define step γ and the tailored regularization coefficient γ and compare them with other methods. A previous study [19] compared the tailored regularization coefficient γ based on the results of several calculations that required considerable time. In this study, step γ is predetermined before the calculation, and the tailored regularization coefficient γ, which is tailored based on the results of several calculations in advance, compares the results with those of methods for a fair comparison.

C. Nondominated-Solution-Based Multiobjective Greedy Algorithm

In this study, we apply an NMG method to solve MOPs with D-optimality for the optimal design of experiments and cost constraints. Algorithm 1 presents the NMG procedure.

As discussed previously, the common greedy method reserves a set of sensors for each step. It determines the best sensor by considering sensor candidates only for a set of sensors obtained in the preceding step and evaluating a single objective function, such as the D-optimality index. The sensor selection procedure is repeated until a particular constraint is satisfied, for instance, when the number of selected sensors k reaches a predefined value p. Similar to the group greedy method, the NMG method evaluates the sensor candidates for $L_{\max}$ sets of sensors obtained in the preceding step. However, it reserves $L_{\max}$ sets of sensors in each step based on the nondominated solutions of the MOP and evaluates the sensor candidates by considering the multiobjective simultaneously. Furthermore, the D-optimality index and the cost constraint defined in (3) and (5) are used as the objective functions considered in the NMG method. In the NMG method, efficient nondominated sorting using the sequential search strategy (ENS-SS) [61] and infinite crowding distance, the relative distances of each solution in the front [53], is used to obtain the nondominated solutions. Nakai et al. [26] provided details on the algorithm for the NMG method. In this study, all NMG calculations are performed with $L_{\max} = 20$ (see the Appendix for a parameter study of $L_{\max}$).

The computational complexities of the DG with cost method and the NMG method for D-optimality for the optimal design of experiments and cost constraints are $\mathcal{O}(pnr^2)$ [13] and $\mathcal{O}(pvn^2r^2L_{\max}^3)$ [26], respectively. Here, v denotes the number of objective functions ($v = 2$ in this study). In the NMG method, the computational complexities for selecting the pth sensor $L_{\max}$ times and sorting using ENS-SS are $\mathcal{O}(pnr^2L_{\max})$ and $\mathcal{O}(vnL_{\max}^2)$, respectively. The computational complexity of the DG method with cost is lower than that of the NMG method; however, the DG method with cost requires a significant adjustment time to determine the tailored regularization coefficient γ before calculation. The multiobjective optimization improves the single-objective results, as demonstrated in previous studies [26], and provides a Pareto solution of the sensor placement value and cost, which aids users in selecting actual sensor placement. While the previously proposed DG method for cost constraints [19] is an empirical formulation with a fixed parameter γ, the NMG method overcomes the empirical formulation and addresses cost constraints in a more natural manner. The NMG method, which performs a multiobjective optimization, has the disadvantage of requiring a higher computational cost than single-objective optimization.

Algorithm 1 NMG Method [26]

Input: p, n, $L_{\max}$
Output: Family of p indices of $L_{\max}$ sets $\mathfrak{S}_p$
Set sensor candidates $\mathcal{S} := \{1, \ldots, n\}$;
$\mathfrak{S}_i \leftarrow \emptyset \ (i \in \{1, \ldots, p\})$;
for $k = 1, \ldots, p$ **do**
  for $l = 1, \ldots, L_{\max}$ **do**
    Calculate objective functions according to Eqs. (3) and (5) for the previously selected l-th group;
  end for
  Eliminate duplication of potential sensor sets;
  $rank \leftarrow 1$;
  while true **do**
    $\mathfrak{F}_k[rank] \leftarrow$ family of sensor sets assigned to $rank$ using ENS-SS;
    $L_k[rank] \leftarrow$ number of sensor sets belonging to $\mathfrak{F}_k[rank]$;
    if $\sum_{i=1}^{rank} L_k[i] \ge L_{\max}$ **then**
      $L'_k = L_{\max} - \sum_{i=1}^{rank-1} L_k[i]$;
      $\Delta\mathfrak{S}_k \leftarrow L'_k$ sets selected using the crowding distance and random selection from $\mathfrak{F}_k[rank]$;
      $\mathfrak{S}_k \leftarrow \mathfrak{S}_k \cup \Delta\mathfrak{S}_k$;
      break;
    else
      $\mathfrak{S}_k \leftarrow \mathfrak{S}_k \cup \mathfrak{F}[rank]$;
      $rank \leftarrow rank + 1$;
    end if
  end while
  $k \leftarrow k + 1$;
end for
return $\mathfrak{S}_p$

D. Datasets

We consider three example datasets: the National Oceanic and Atmospheric Administration Optimum Interpolation Sea Surface Temperature (NOAA OISST) V2 mean sea surface temperature set, the velocity field around NACA0015 measured by particle image velocimetry (PIV), and the brightness from the direct measurement of a rocket combustion chamber. A proper orthogonal decomposition (POD) [62], [63]

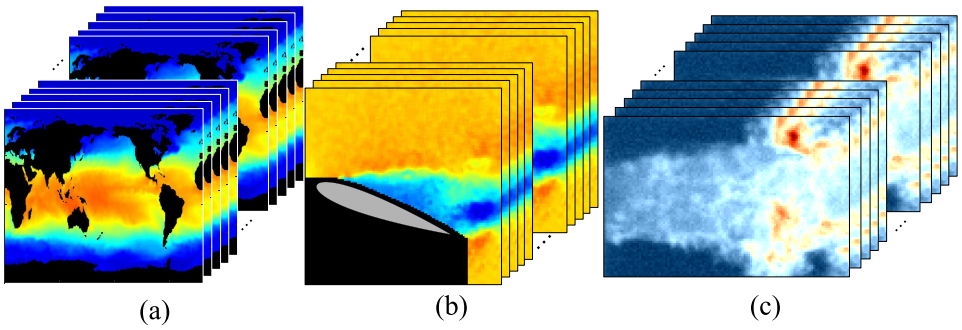

Fig. 1. Three datasets considered in this study: snapshots of (a) global sea surface temperature, (b) flowfield around an airfoil, and (c) combustion field in a rocket combustion chamber.

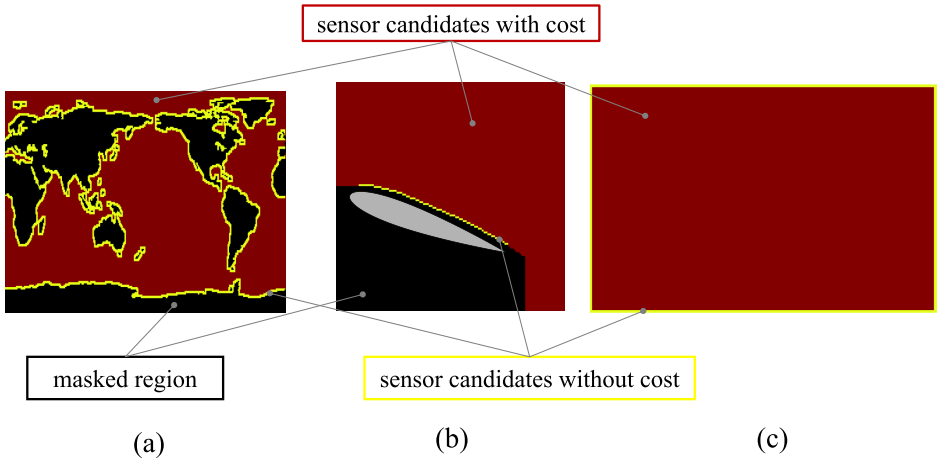

Fig. 2. Cost functions used in this study: (a) global sea surface temperature, (b) flowfield around an airfoil, and (c) combustion field in a rocket combustion chamber. Black, yellow, and red indicate regions of the mask, zero cost, and unity cost, respectively.

is applied to the data matrix $\mathbf{X} \in \mathbb{R}^{n\times m}$, which comprises m snapshots with spatial dimension n, and a reduced-order model is predefined by the first r low-order POD modes. Here, the dimensions of the data matrix are reduced to $r = 10$.

Snapshot examples and cost functions for each system are shown in Figs. 1 and 2. The black, yellow, and red regions shown in Fig. 2 indicate the mask, zero, and unity costs, respectively. The cost function used in this study is a binary function with only zero or unity costs. This simplified cost function was employed in a previous study [19].

The first case employed the NOAA OISST (NOAA-SST) V2 mean sea surface temperature dataset, comprising weekly global sea surface temperature measurements from 1990 to 2000. The data are available online [64]. The data were generated weekly on a 1 ° grid and used in situ with satellite data, along with data simulated for the sea ice cover. There were 520 snapshots on a 360 × 180 spatial grid [Fig. 1(a)]. The size of the data matrix was $\mathbf{X} \in \mathbb{R}^{44\,219\times 520}$. The binary cost function in NOAA-SST is zero for locations one and two pixels off land and equal to one everywhere else, as shown in Fig. 2(a). This cost function was employed in a previous study [19] and is a set of cost functions based on the idea that sensors (e.g., a buoy) are easier to install in the sea close to land, but more difficult to install away from land.

The second case adopted a time-resolved dataset of the velocity field around an airfoil acquired by a previously obtained PIV measurement [65] [Fig. 1(b)]. The wind-tunnel tests were performed in a small low-turbulence wind tunnel at the Institute of Fluid Science, Tohoku University, Sendai, Japan. The airfoil of the test model had an NACA0015 profile, and the chord length and the span width were 100 and 300 mm, respectively. The freestream velocity U_∞ and the attack angle of the airfoil α were set as 10 m/s and 18°, respectively. The spatial resolution was set to 1024 × 1024 pixels. The size of the data matrix was $\mathbf{X} \in \mathbb{R}^{9353\times 10\,000}$. The binary cost function in the velocity field is zero for the locations of one pixel of the mask on the airfoil surface and is equal to one elsewhere, as shown in Fig. 2(b). A hot-wire anemometer or similar device can obtain the spatial velocity; however, the location and fixation of the device are extremely difficult. On the other hand, it is relatively easy to measure the velocity field using a pressure sensor embedded in an airfoil on the surface. The combustion field in a rocket chamber has the same problem as the flow field around the airfoil.

These ideas led to the problem settings of the flow field around the airfoil and the combustion field in the rocket chamber with the cost functions shown in Fig. 2(b) and (c). The third case utilizes a time-resolved dataset of the combustion field of a liquid rocket engine obtained by Sakaki et al. [66] [Fig. 1(c)]. It is extremely important to ensure combustion

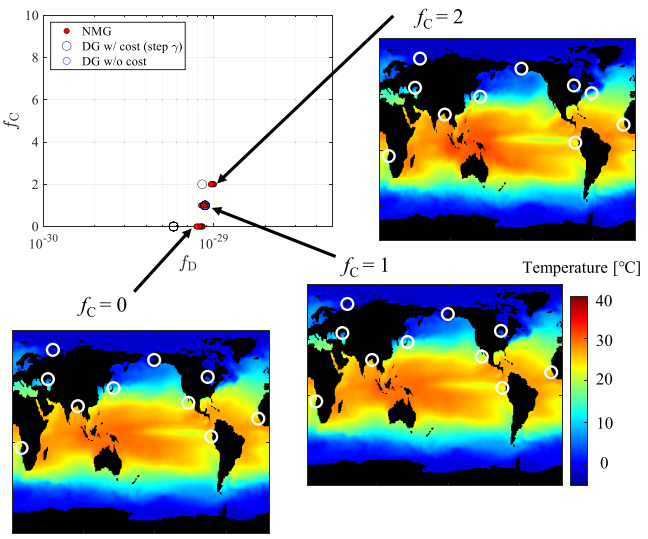

Fig. 3. Relationship between f_D and f_C for $r = 10$, $p = 10$, and $L_{max} = 20$ in the case of NOAA-SST. Step γ is set to $\gamma \in [0, 10^{-9}, 10^{-8}, \ldots, 10^{8}, 10^{9}]$. Single snapshots were reconstructed by the NMG method in each f_C. The open circles show the selected sensor position.

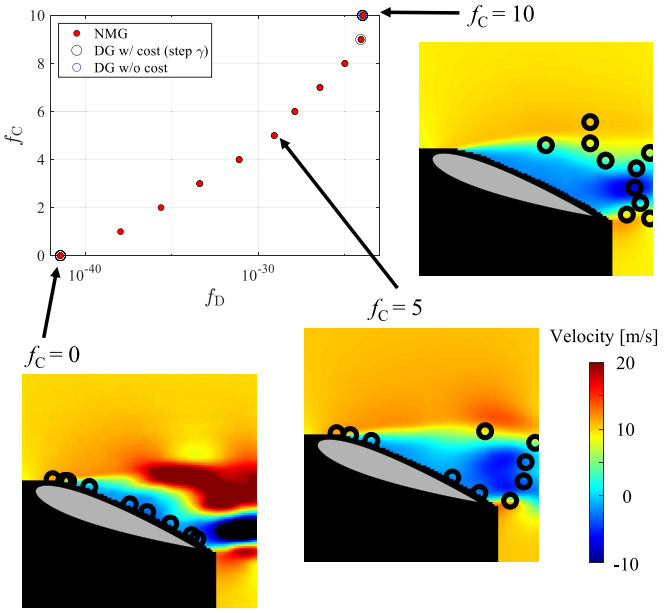

Fig. 4. Relationship between f_D and f_C for $r = 10$, $p = 10$, and $L_{max} = 20$ in the case of a flowfield the around airfoil. Step γ is set to $\gamma \in [0, 10^{-9}, 10^{-8}, \ldots, 10^{8}, 10^{9}]$. Single snapshots were reconstructed by the NMG method in each f_C. The open circles show the selected sensor position.

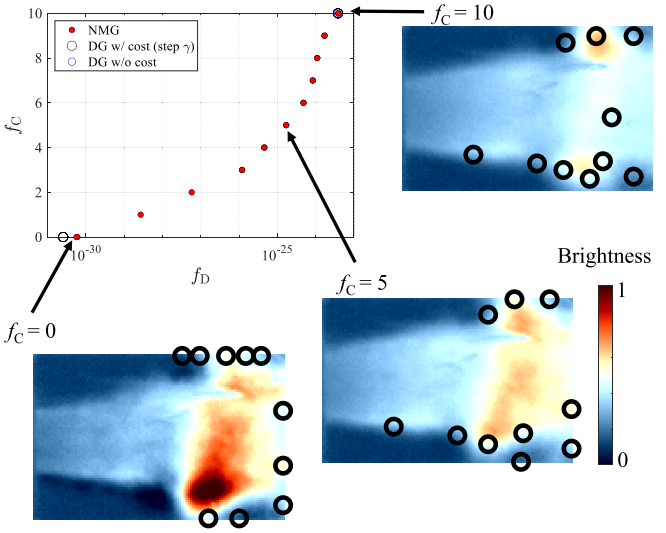

Fig. 5. Relationship between f_D and f_C for $r = 10$, $p = 10$, and $L_{max} = 20$ in the case of the combustion field in the rocket chamber. Step γ is set to $\gamma \in [0, 10^{-9}, 10^{-8}, \ldots, 10^{8}, 10^{9}]$. Single snapshots were reconstructed by the NMG method in each f_C. The open circles show the selected sensor position.

stability in rocket engines. The mechanisms of combustion instability or oscillation are not well understood. Therefore, visualization of unsteady combustion behavior using a high-speed camera is an effective tool for understanding the fundamental phenomena of combustion instability. It is possible to investigate this essential phenomenon by extracting characteristic behaviors from a large amount of visualization data [67]. Anomaly detection can be performed efficiently by sparsely measuring the extracted characteristic behaviors. The combustion field in the hydrogen–oxygen rocket chamber was mainly the water vapor emission intensity due to the temperature of the combustion gas. The size of the data matrix was $\mathbf{X} \in \mathbb{R}^{8550 \times 1001}$. The binary cost function in the combustion field is zero for locations one pixel off the rim of the field and is equal to one everywhere else, as shown in Fig. 2(c).

III. Results and Discussion

A. Comparison of Each Method: NMG, DG w/, and DG w/o Cost (Step γ)

Figs. 3–5 show the relationship between f_D and f_C for $r = 10$, $p = 10$, and $L_{max} = 20$ in NOAA-SST, the flowfield around the airfoil, and the combustion field in the rocket chamber, respectively. The red-closed, black-open, and blue-open circles represent the results obtained using sensors selected by the NMG method, the DG method w/ cost (step γ), and the DG method w/o cost, respectively. Here, the step γ is set to $\gamma \in [0, 10^{-9}, 10^{-8}, \ldots, 10^{8}, 10^{9}]$. In addition, in Figs. 3–5, each snapshot is reconstructed using the NMG method for each f_C value. Fig. 6 shows the relationship between f_D and f_C for $r = 10$ and $p = 20$ at $L_{max} = 20$ for NOAA-SST, flowfield around the airfoil, and combustion field in the rocket chamber, respectively. All the optimization directions in the objective-function space shown in Figs. 3–6 are at the bottom right; thus, the sensors selected by the sensor selection method are inexpensive and highly accurate.

In the case of NOAA-SST, as shown in Figs. 3 and 6(a), a Pareto front is expected to exist with a cost ranging from 0 to p; however, the results in NOAA-SST have Pareto fronts of $0 \leq f_C \leq 2$ for undersampling and $0 \leq f_C \leq 4$ for oversampling. This indicates that valuable locations in terms of improving the estimation accuracy exist around the land, where the cost is equal to zero. The Pareto front obtained by the NMG method was better than that obtained by the DG method with respect to the cost of NOAA-SST.

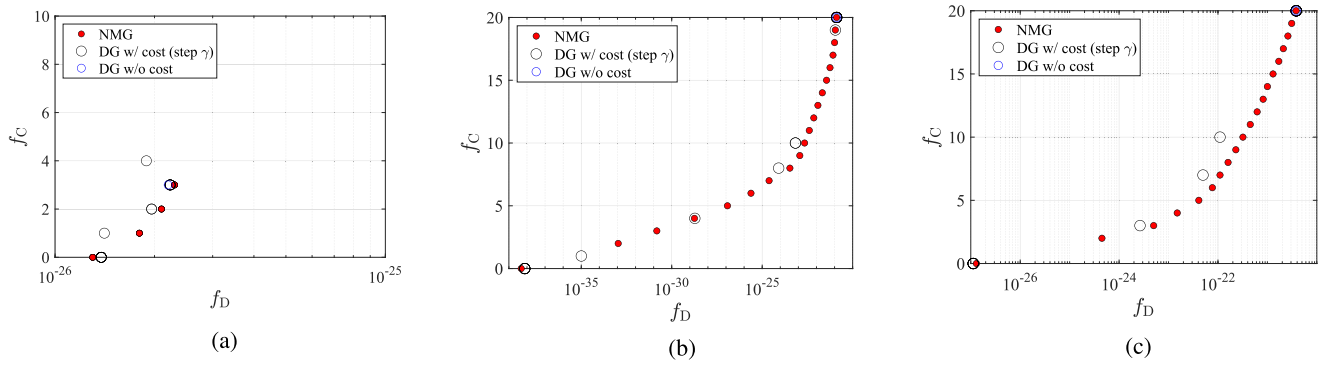

Fig. 6. Relationship between f_D and f_C for $r = 10$ and $L_{max} = 20$. Step γ is set to $\gamma \in [0, 10^{-9}, 10^{-8}, \ldots, 10^{8}, 10^{9}]$. (a) NOAA-SST in the oversampling case ($p = 20$). (b) Flowfield around the airfoil in the oversampling case ($p = 20$). (c) Combustion field in the rocket chamber in the oversampling case ($p = 20$).

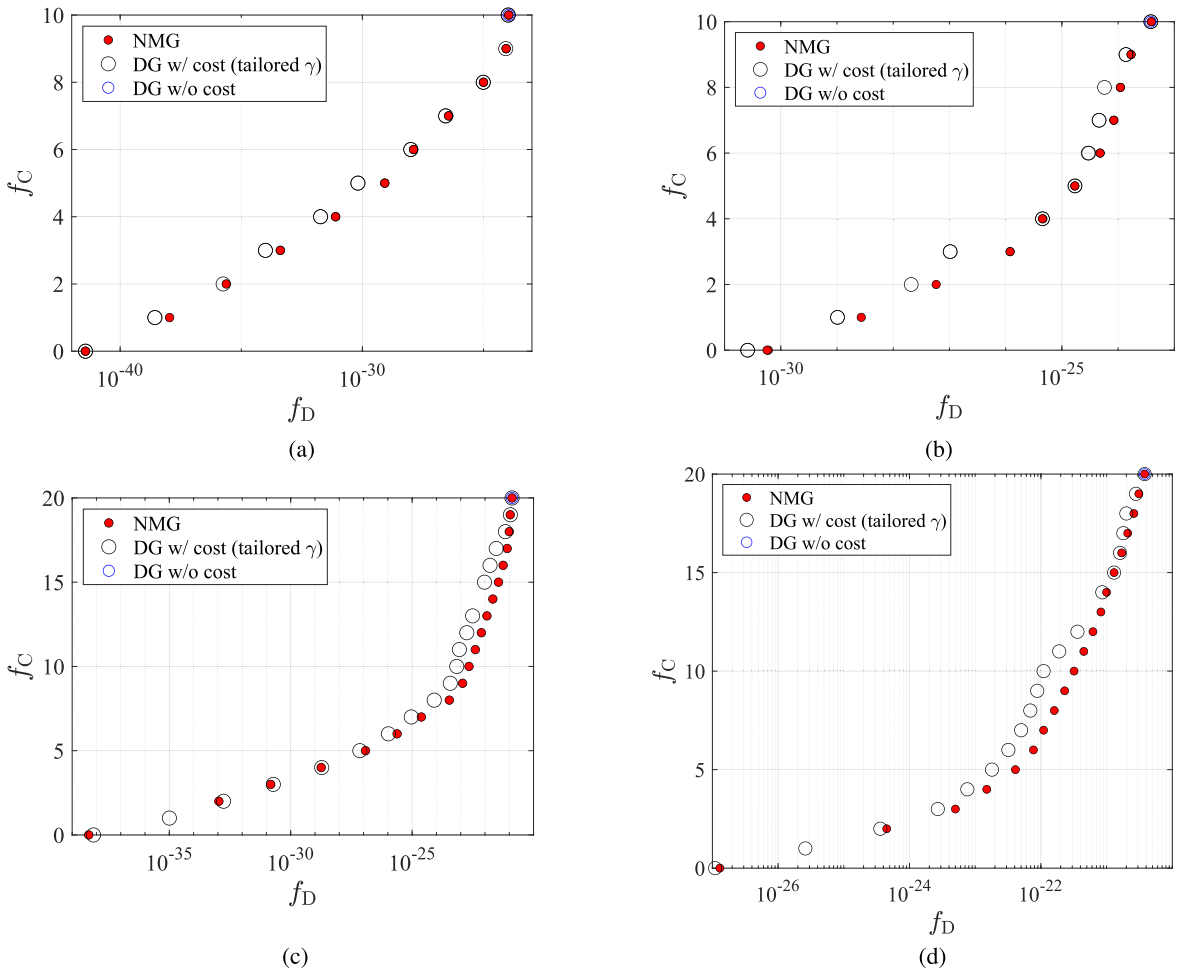

Fig. 7. Relationship between f_D and f_C for $r = 10$ and $L_{max} = 20$. The tailored regularization coefficient γ was used for the DG method w/ cost. (a) Velocity field around the airfoil in the undersampling case ($p = 10$). (b) Combustion field in the rocket chamber in the undersampling case ($p = 10$). (c) Velocity field around the airfoil in the oversampling case ($p = 20$). (d) Combustion field in the rocket chamber in the oversampling case ($p = 20$).

In the case of the flow and combustion fields, as shown in Figs. 4, 5, and 6(b) and (c), unlike the NOAA-SST results, the NMG method has a Pareto front with $0 \leq f_C \leq p$. Because the NMG method can obtain a continuous Pareto front, it is easy to select a sensor set that satisfies the cost requirements. In contrast, the DG method w/ cost is an intermittent Pareto front. This is because the fixed parameter γ is not adjusted for these calculations, and step γ overlaps with the solution.

B. Comparison of Each Method: NMG, DG w/, and DG w/o Cost (Tailored Regularization Coefficient γ)

The results obtained by the DG method w/ cost using the step γ overlap resulted in an intermittent Pareto front.

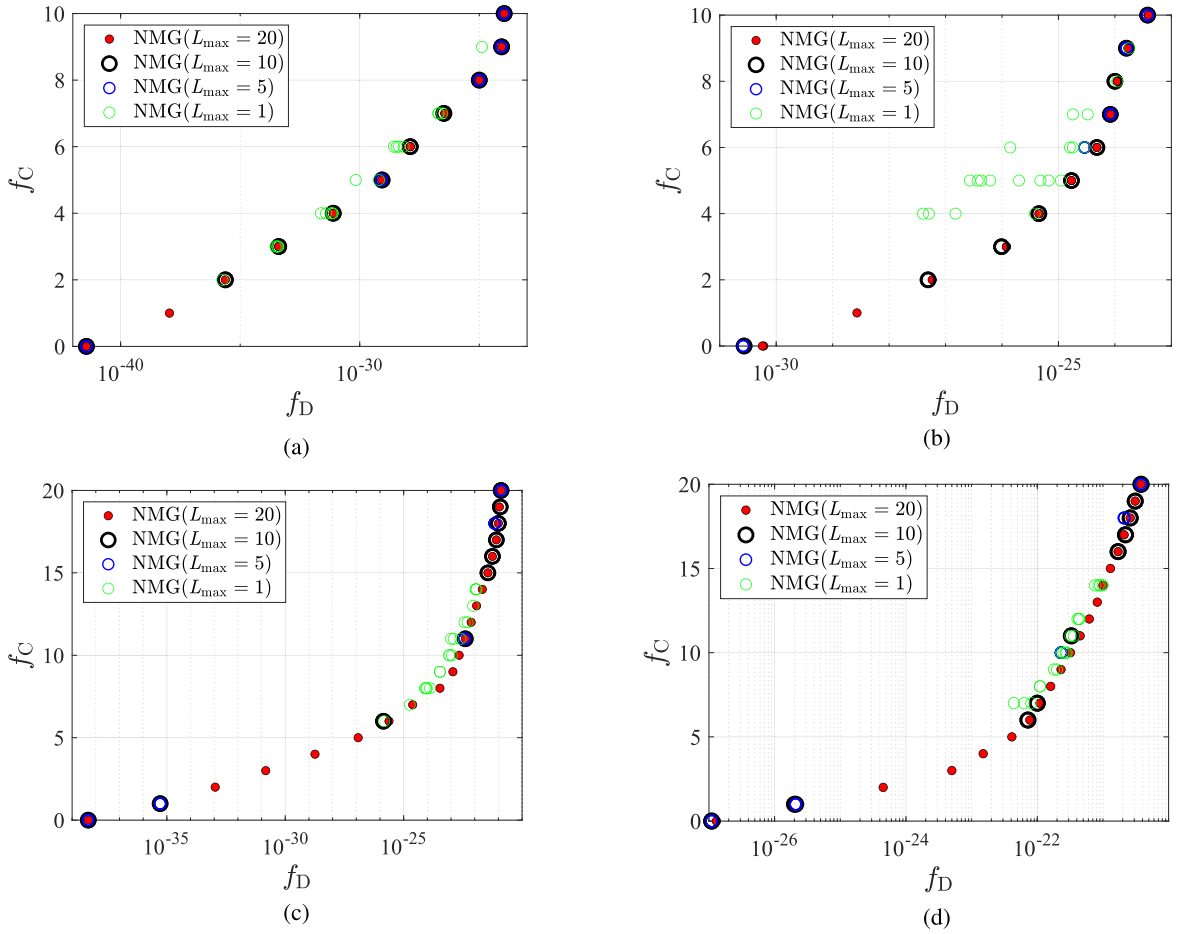

Fig. 8. Relationship between f_D and f_C for $r = 10$ and $L_{\max} = 1, 5, 10$, and 20. (a) Velocity field around the airfoil in the undersampling case ($p = 10$). (b) Combustion field in the rocket chamber in the undersampling case ($p = 10$). (c) Velocity field around the airfoil in the oversampling case ($p = 20$). (d) Combustion field in the rocket chamber in the oversampling case ($p = 20$).

Therefore, this study introduces a tailored regularization coefficient γ based on several precalculations, and the results obtained by the DG method w/ cost using the tailored regularization coefficient γ are compared with those obtained by the NMG method.

Fig. 7 shows the relationship between f_D and f_C for $r = 10$ and $L_{\max} = 20$. Here, the tailored regularization coefficient γ is used for the DG method w/ cost. Table I lists the used tailored regularization coefficient γ. Note that the tailored regularization coefficient γ was obtained from several precalculations and was time-consuming.

As shown in Fig. 7, the results obtained by the DG method w/ cost using the tailored regularization coefficient γ also exhibit continuous Pareto fronts in the undersampling and oversampling cases. Comparing f_D for each f_C, the NMG method may rarely be slightly worse than the DG w/cost method; however, in most cases, the NMG method is superior to the DG w/cost method.

Finally, it should be noted that this study only considers problems with a binary cost function for the sensors and that the proposed method works significantly in such cases. However, the performance of the NMG method is degraded if we consider the continuous cost function, which has a different cost for each sensor. This is because the continuous cost function often leads to a large number of nondominated solutions that are larger than the hyperparameter of L in this study, and a random selection embedded in this algorithm of nondominated solutions becomes key. We applied the NMG method to this problem; however, the performance seemed to degrade. The scope of this study is the application of the NMG method to almost the same problem setting as

TABLE I
TAILORED REGULARIZATION COEFFICIENT γ FOR THE DG METHOD W/ COST

	Flow field around an airfoil	Temperature field in a rocket chamber
Undersampling	$\gamma \in$ [0, 0.0001, 0.003, 0.04, 0.05, 0.052, 0.0525, 0.053 0.0535, 0.054, 0.0541, 0.055, 0.056, 0.06, 0.063, 0.065, 0.072, 0.075, 0.084, 0.1]	$\gamma \in$ [0, 0.001, 0.015, 0.016, 0.0164, 0.0165, 0.017, 0.0175 0.018, 0.02, 0.022, 0.037, 0.038, 0.0383, 0.0384, 0.04, 0.05, 0.053, 0.06, 0.1]
Oversampling	$\gamma \in$ [0, 0.0001, 0.003, 0.04, 0.05, 0.052, 0.0525, 0.053 0.0535, 0.054, 0.0541, 0.055, 0.056, 0.06, 0.063, 0.065, 0.072, 0.075, 0.084, 0.1]	$\gamma \in$ [0, 0.015, 0.016, 0.017, 0.018, 0.02, 0.038, 0.04, 0.05, 0.1, 0.45, 0.5, 0.8, 1.3, 1.5, 3, 5, 35, 88, 100]

the cost-constrained sensor problem with a stepwise cost function as that in the previous study, which should be further investigated in future studies.

IV. Conclusion

In this study, a new greedy sensor selection algorithm with a cost constraint was proposed based on the NMG method, and its performance was investigated by comparing it with a previously proposed method. The cost function was simultaneously considered using the D-optimality criterion, and the sensor set was selected based on the idea of a nondominated solution. We demonstrated the effectiveness of the proposed algorithm on three different real datasets related to the sea surface temperature field, the flowfield around an airfoil, and the combustion field in a rocket chamber. A binary cost function was virtually imposed for each potential sensor location, and a sensor selection problem with a cost constraint was simulated. The results of numerical experiments demonstrated that the NMG method can yield a Pareto solution. Introducing a tailored regularization coefficient obtained by multiple precalculations improves the results of the previous method; however, the objective values of almost all sensors set at certain costs selected by the proposed method are superior to those selected by the previous method.

Appendix
Parameter Study: $L_{\max}$

A parameter study is conducted on $L_{\max}$. The NMG method reserves $L_{\max}$ sets of sensors in each step based on the nondominated solutions of the MOP and evaluates the sensor candidates by considering the multiobjective simultaneously. Therefore, a parameter study on the function of $L_{\max}$ in the NMG method can be performed by calculating the NMG method with several $L_{\max}$. All calculations in this study were performed with $L_{\max} = 20$. Therefore, the parameter study is performed with the number of calculations N changed so that the computational cost is the same condition as for $L_{\max} = 20$: $N = 1$ for $L_{\max} = 20$, $N = 2$ for $L_{\max} = 10$, $N = 4$ for $L_{\max} = 5$, and $N = 20$ for $L_{\max} = 1$. Fig. 8 shows the relationship between f_{D} and f_{C} for $r = 10$, $p = 10$, and $p = 20$, in the flowfield around the airfoil, and the combustion field in the rocket chamber. The red-closed, black-open, blue-open, and green-open circles represent the results obtained using sensors selected by the NMG method for $L_{\max} = 20$, $L_{\max} = 10$, $L_{\max} = 5$, and $L_{\max} = 1$, respectively. For both calculations with equal computational cost, the results for $L_{\max} = 1$ are close to those of $L_{\max} = 20$; however, the Pareto front is $L_{\max} = 20$ for all results. These results typically demonstrate that it is more Pareto front to consider a multiobjective ($L_{\max} > 1$) than a single objective ($L_{\max} = 1$). A Pareto front can be obtained by increasing $L_{\max}$. Regarding $L_{\max} = 20$, a Pareto front exists with a cost ranging from 0 to p approximately. Therefore, the NMG method was performed under the condition of $L_{\max} = 20$ in this study.

References

[1] W. A. Maul, G. Kopasakis, L. M. Santi, T. S. Sowers, and A. Chicatelli, "Sensor selection and optimization for health assessment of aerospace systems," *J. Aerosp. Comput., Inf., Commun.*, vol. 5, no. 1, pp. 16–34, Jan. 2008, doi: 10.2514/1.34677.

[2] N. Omata, D. Satoh, S. Tsutsumi, K. Kawatsu, and M. Abe, "Model-based supervised sensor placement optimization to detect propellant leak in a liquid rocket engine," *Acta Astronautica*, vol. 195, pp. 234–242, Jun. 2022.

[3] A. Atkinson et al., *Optimum Experimental Designs, With SAS*, vol. 34. Oxford, U.K.: Oxford Univ. Press, 2007.

[4] S. Joshi and S. Boyd, "Sensor selection via convex optimization," *IEEE Trans. Signal Process.*, vol. 57, no. 2, pp. 451–462, Feb. 2009.

[5] T. Nonomura, S. Ono, K. Nakai, and Y. Saito, "Randomized subspace Newton convex method applied to data-driven sensor selection problem," *IEEE Signal Process. Lett.*, vol. 28, pp. 284–288, 2021.

[6] F. Lin, M. Fardad, and M. R. Jovanovic, "Design of optimal sparse feedback gains via the alternating direction method of multipliers," *IEEE Trans. Autom. Control*, vol. 58, no. 9, pp. 2426–2431, Sep. 2013.

[7] M. Fardad, F. Lin, and M. R. Jovanovic, "Sparsity-promoting optimal control for a class of distributed systems," in *Proc. Amer. Control Conf.*, Jun. 2011, pp. 2050–2055.

[8] N. K. Dhingra, M. R. Jovanovic, and Z.-Q. Luo, "An ADMM algorithm for optimal sensor and actuator selection," in *Proc. 53rd IEEE Conf. Decis. Control*, Dec. 2014, pp. 4039–4044.

[9] A. Zare and M. R. Jovanovic, "Optimal sensor selection via proximal optimization algorithms," in *Proc. IEEE Conf. Decis. Control (CDC)*, Dec. 2018, pp. 6514–6518.

[10] T. Nagata, T. Nonomura, K. Nakai, K. Yamada, Y. Saito, and S. Ono, "Data-driven sparse sensor selection based on A-optimal design of experiment with ADMM," *IEEE Sensors J.*, vol. 21, no. 13, pp. 15248–15257, Jul. 2021.

[11] T. Nagata, K. Yamada, T. Nonomura, K. Nakai, Y. Saito, and S. Ono, "Data-driven sensor selection method based on proximal optimization for high-dimensional data with correlated measurement noise," *IEEE Trans. Signal Process.*, vol. 70, pp. 5251–5264, 2022.

[12] K. Manohar, B. W. Brunton, J. N. Kutz, and S. L. Brunton, "Data-driven sparse sensor placement for reconstruction: Demonstrating the benefits of exploiting known patterns," *IEEE Control Syst. Mag.*, vol. 38, no. 3, pp. 63–86, Jun. 2018.

[13] Y. Saito et al., "Determinant-based fast greedy sensor selection algorithm," *IEEE Access*, vol. 9, pp. 68535–68551, 2021.

[14] Y. Saito et al., "Data-driven vector-measurement-sensor selection based on greedy algorithm," *IEEE Sensors Lett.*, vol. 4, no. 7, pp. 1–4, Jul. 2020.

[15] K. Nakai, K. Yamada, T. Nagata, Y. Saito, and T. Nonomura, "Effect of objective function on data-driven greedy sparse sensor optimization," *IEEE Access*, vol. 9, pp. 46731–46743, 2021.

[16] J. Ranieri, A. Chebira, and M. Vetterli, "Near-optimal sensor placement for linear inverse problems," *IEEE Trans. Signal Process.*, vol. 62, no. 5, pp. 1135–1146, Mar. 2014.

[17] C. Jiang, Y. C. Soh, and H. Li, "Sensor placement by maximal projection on minimum eigenspace for linear inverse problems," *IEEE Trans. Signal Process.*, vol. 64, no. 21, pp. 5595–5610, Nov. 2016.

[18] M. Shamaiah, S. Banerjee, and H. Vikalo, "Greedy sensor selection: Leveraging submodularity," in *Proc. 49th IEEE Conf. Decis. Control (CDC)*, Dec. 2010, pp. 2572–2577.

[19] E. Clark, T. Askham, S. L. Brunton, and J. Nathan Kutz, "Greedy sensor placement with cost constraints," *IEEE Sensors J.*, vol. 19, no. 7, pp. 2642–2656, Apr. 2019.

[20] K. Manohar, J. N. Kutz, and S. L. Brunton, "Optimal sensor and actuator selection using balanced model reduction," *IEEE Trans. Autom. Control*, vol. 67, no. 4, pp. 2108–2115, Apr. 2022.

[21] S. Chaturantabut and D. C. Sorensen, "Nonlinear model reduction via discrete empirical interpolation," *SIAM J. Sci. Comput.*, vol. 32, no. 5, pp. 2737–2764, Jan. 2010.

[22] K. Yamada, Y. Saito, K. Nankai, T. Nonomura, K. Asai, and D. Tsubakino, "Fast greedy optimization of sensor selection in measurement with correlated noise," *Mech. Syst. Signal Process.*, vol. 158, Sep. 2021, Art. no. 107619. [Online]. Available: https://www.sciencedirect.com/science/article/pii/S0888327021000145

[23] T. Inoue et al., "Data-driven optimal sensor placement for high-dimensional system using annealing machine," *Mech. Syst. Signal Process.*, vol. 188, Apr. 2023, Art. no. 109957.

[24] K. Yamada, Y. Saito, T. Nonomura, and K. Asai, "Greedy sensor selection for weighted linear least squares estimation under correlated noise," *IEEE Access*, vol. 10, pp. 79356–79364, 2022.

[25] B. Li, H. Liu, and R. Wang, "Efficient sensor placement for signal reconstruction based on recursive methods," *IEEE Trans. Signal Process.*, vol. 69, pp. 1885–1898, 2021.

[26] K. Nakai, Y. Sasaki, T. Nagata, K. Yamada, Y. Saito, and T. Nonomura, "Nondominated-solution-based multi-objective greedy sensor selection for optimal design of experiments," *IEEE Trans. Signal Process.*, vol. 70, pp. 5694–5707, 2022.

[27] T. Nagata, K. Yamada, K. Nakai, Y. Saito, and T. Nonomura, "Randomized group-greedy method for large-scale sensor selection problems," *IEEE Sensors J.*, vol. 23, no. 9, pp. 9536–9548, May 2023.

[28] K. Yamada, Y. Sasaki, T. Nagata, K. Nakai, D. Tsubakino, and T. Nonomura, "Efficient sensor node selection for observability Gramian optimization," *Sensors*, vol. 23, no. 13, p. 5961, Jun. 2023. [Online]. Available: https://www.mdpi.com/1424-8220/23/13/5961

[29] S. Takahashi et al., "Sensor selection by greedy method for linear dynamical systems: Comparative study on Fisher-information-matrix, observability-Gramian and Kalman-filter-based indices," *IEEE Access*, vol. 11, pp. 67850–67864, 2023.

[30] N. Kanda, K. Nakai, Y. Saito, T. Nonomura, and K. Asai, "Feasibility study on real-time observation of flow velocity field using sparse processing particle image velocimetry," *Trans. Jpn. Soc. Aeronaut. Space Sci.*, vol. 64, no. 4, pp. 242–245, 2021.

[31] S. Kaneko et al., "Data-driven sparse sampling for reconstruction of acoustic-wave characteristics used in aeroacoustic beamforming," *Appl. Sci.*, vol. 11, no. 9, p. 4216, May 2021.

[32] T. Inoue, Y. Matsuda, T. Ikami, T. Nonomura, Y. Egami, and H. Nagai, "Data-driven approach for noise reduction in pressure-sensitive paint data based on modal expansion and time-series data at optimally placed points," *Phys. Fluids*, vol. 33, no. 7, Jul. 2021, Art. no. 077105, doi: 10.1063/5.0049071.

[33] B. Li, H. Liu, and R. Wang, "Data-driven sensor placement for efficient thermal field reconstruction," *Sci. China Technol. Sci.*, vol. 64, no. 9, pp. 1981–1994, Sep. 2021.

[34] D. W. Carter, F. De Voogt, R. Soares, and B. Ganapathisubramani, "Data-driven sparse reconstruction of flow over a stalled aerofoil using experimental data," *Data-Centric Eng.*, vol. 2, p. e5, Jan. 2021.

[35] N. Kanda et al., "Proof-of-concept study of sparse processing particle image velocimetry for real time flow observation," *Experim. Fluids*, vol. 63, no. 9, p. 143, Sep. 2022.

[36] W.-J. Yeo, S. Taulu, and J. N. Kutz, "Effcient magnetometer sensor array selection for signal reconstruction and brain source localization," 2022, *arXiv:2205.10925*.

[37] R. Inoba et al., "Optimization of sparse sensor placement for estimation of wind direction and surface pressure distribution using time-averaged pressure-sensitive paint data on automobile model," *J. Wind Eng. Ind. Aerodyn.*, vol. 227, Aug. 2022, Art. no. 105043.

[38] T. Nagata et al., "Seismic wavefield reconstruction based on compressed sensing using data-driven reduced-order model," *Geophys. J. Int.*, vol. 233, no. 1, pp. 33–50, Aug. 2022.

[39] G. Jiang, M. Kang, Z. Cai, H. Wang, Y. Liu, and W. Wang, "Online reconstruction of 3D temperature field fused with POD-based reduced order approach and sparse sensor data," *Int. J. Thermal Sci.*, vol. 175, May 2022, Art. no. 107489.

[40] N. Tiwari, K. Uchida, R. Inoba, Y. Saito, K. Asai, and T. Nonomura, "Simultaneous measurement of pressure and temperature on the same surface by sensitive paints using the sensor selection method," *Experim. Fluids*, vol. 63, no. 11, pp. 1–13, Nov. 2022.

[41] K. Nakai et al., "Observation site selection for physical model parameter estimation towards process-driven seismic wavefield reconstruction," *Geophys. J. Int.*, vol. 234, no. 3, pp. 1786–1805, Apr. 2023, doi: 10.1093/gji/ggad165.

[42] N. Tiwari, "Ultrasonic velocity profiler placement for flow over cylinder based on determinant greedy line selection method," *Experim. Fluids*, vol. 64, no. 6, Jun. 2023.

[43] H. Peng, S. Si, M. K. Awad, N. Zhang, H. Zhao, and X. S. Shen, "Toward energy-efficient and robust large-scale WSNs: A scale-free network approach," *IEEE J. Sel. Areas Commun.*, vol. 34, no. 12, pp. 4035–4047, Dec. 2016.

[44] X. Fu, P. Pace, G. Aloi, L. Yang, and G. Fortino, "Topology optimization against cascading failures on wireless sensor networks using a memetic algorithm," *Comput. Netw.*, vol. 177, Aug. 2020, Art. no. 107327.

[45] X. Fu, P. Pace, G. Aloi, W. Li, and G. Fortino, "Toward robust and energy-efficient clustering wireless sensor networks: A double-stage scale-free topology evolution model," *Comput. Netw.*, vol. 200, Dec. 2021, Art. no. 108521.

[46] J. Yan, H. Liu, W. Pu, S. Zhou, Z. Liu, and Z. Bao, "Joint beam selection and power allocation for multiple target tracking in netted colocated MIMO radar system," *IEEE Trans. Signal Process.*, vol. 64, no. 24, pp. 6417–6427, Dec. 2016.

[47] Z. Li, J. Xie, H. Zhang, H. Xiang, and C. Wang, "Joint beam selection and resource allocation for cognitive multiple targets tracking in MIMO radar with collocated antennas," *IET Radar, Sonar Navigat.*, vol. 14, no. 12, pp. 2000–2009, Dec. 2020.

[48] J. Yan, H. Jiao, W. Pu, C. Shi, J. Dai, and H. Liu, "Radar sensor network resource allocation for fused target tracking: A brief review," *Inf. Fusion*, vols. 86–87, pp. 104–115, Oct. 2022.

[49] M. Xie, W. Yi, T. Kirubarajan, and L. Kong, "Joint node selection and power allocation strategy for multitarget tracking in decentralized radar networks," *IEEE Trans. Signal Process.*, vol. 66, no. 3, pp. 729–743, Feb. 2018.

[50] G. Yu, H. Fu, and Y. Liu, "High-dimensional cost-constrained regression via nonconvex optimization," *Technometrics*, vol. 64, no. 1, pp. 1–13, 2021.

[51] J. Horn, N. Nafpliotis, and D. E. Goldberg, "A niched Pareto genetic algorithm for multiobjective optimization," in *Proc. 1st IEEE Conf. Evol. Comput., IEEE World Congr. Comput. Intell.*, Mar. 1994, pp. 82–87.

[52] N. Srinivas and K. Deb, "Muiltiobjective optimization using nondominated sorting in genetic algorithms," *Evol. Comput.*, vol. 2, no. 3, pp. 221–248, Sep. 1994.

[53] K. Deb, A. Pratap, S. Agarwal, and T. Meyarivan, "A fast and elitist multiobjective genetic algorithm: NSGA-II," *IEEE Trans. Evol. Comput.*, vol. 6, no. 2, pp. 182–197, Apr. 2002.

[54] K. Shimoyama, S. Yoshimizu, S. Jeong, S. Obayashi, and Y. Yokono, "Multi-objective design optimization for a steam turbine stator blade using LES and GA," *J. Comput. Sci. Technol.*, vol. 5, no. 3, pp. 134–147, 2011.

[55] Z. Liu, L. Dong, J.-M. Moschetta, J. Zhao, and G. Yan, "Optimization of nano-rotor blade airfoil using controlled elitist NSGA-II," *Int. J. Micro Air Vehicles*, vol. 6, no. 1, pp. 29–42, Mar. 2014, doi: 10.1260/1756-8293.6.1.29.

[56] J.-H. Jeong and S.-H. Kim, "Optimization of thick wind turbine airfoils using a genetic algorithm," *J. Mech. Sci. Technol.*, vol. 32, no. 7, pp. 3191–3199, Jul. 2018.

[57] X. Wei, X. Wang, and S. Chen, "Research on parameterization and optimization procedure of low-Reynolds-number airfoils based on genetic algorithm and Bezier curve," *Adv. Eng. Softw.*, vol. 149, Jan. 2020, Art. no. 102864. [Online]. Available: https://www.sciencedirect.com/science/article/pii/S0965997820303045

[58] C. Jiang, Z. Chen, R. Su, and Y. C. Soh, "Group greedy method for sensor placement," *IEEE Trans. Signal Process.*, vol. 67, no. 9, pp. 2249–2262, May 2019.

[59] J. Kennedy and R. C. Eberhart, "Particle swarm optimization," in *Proc. IEEE Int. Conf. Neural Netw.*, vol. 4, May 1995, pp. 1942–1948.

[60] M. Dorigo, V. Maniezzo, and A. Colorni, "Ant system: Optimization by a colony of cooperating agents," *IEEE Trans. Syst., Man, Cybern., B, Cybern.*, vol. 26, no. 1, pp. 29–41, Feb. 1996.

[61] X. Zhang, Y. Tian, R. Cheng, and Y. Jin, "An efficient approach to nondominated sorting for evolutionary multiobjective optimization," *IEEE Trans. Evol. Comput.*, vol. 19, no. 2, pp. 201–213, Apr. 2015.

[62] G. Berkooz, P. Holmes, and J. L. Lumley, "The proper orthogonal decomposition in the analysis of turbulent flows," *Annu. Rev. Fluid Mech.*, vol. 25, no. 1, pp. 539–575, Jan. 1993.

[63] K. Taira et al., "Modal analysis of fluid flows: An overview," *AIAA J.*, vol. 55, no. 12, pp. 4013–4041, Dec. 2017.

[64] NOAA/OAR/ESRL. *NOAA Optimal Interpolation (OI) Sea Surface Temperature (SST) V2*. Accessed: Apr. 2, 2020. [Online]. Available: https://www.esrl.noaa.gov/psd/data/gridded/data.noaa.oisst.v2.html

[65] T. Nonomura, K. Nankai, Y. Iwasaki, A. Komuro, and K. Asai, "Quantitative evaluation of predictability of linear reduced-order model based on particle-image-velocimetry data of separated flow field around airfoil," *Experim. Fluids*, vol. 62, no. 5, p. 112, May 2021.

[66] K. Sakaki, Y. Nunome, and T. Tomita, "Optical measurement for injection-coupled unsteady combustion behaviors of a shear coaxial injector in liquid oxygen/hydrogen rocket engine combustor," *J. Jpn. Soc. Aeronaut. Space Sci.*, vol. 68, no. 2, pp. 72–81, 2020.

[67] K. Sakaki et al., "Longitudinal combustion instability of a pintle injector for a liquid rocket engine combustor," *Combustion Flame*, vol. 194, pp. 115–127, Aug. 2018.

Yuji Saito received the B.S. degree in mechanical engineering and the M.S. and Ph.D. degrees in mechanical space engineering from Hokkaido University, Sapporo, Japan, in 2014, 2016, and 2018, respectively.

From 2017 to 2018, he was a Research Fellow of the Japan Society for the Promotion of Science (JSPS) at Hokkaido University. He is currently an Assistant Professor at the Frontier Research Institute for Interdisciplinary Sciences, Tohoku University, Sendai, Japan.

Kumi Nakai received the Ph.D. degree in mechanical systems engineering from the Tokyo University of Agriculture and Technology, Tokyo, Japan, in 2020.

From 2017 to 2020, she was a Research Fellow of the Japan Society for the Promotion of Science (JSPS) at the Tokyo University of Agriculture and Technology. She is currently a Researcher with the National Institute of Advanced Industrial Science and Technology, Tsukuba, Japan.

Takayuki Nagata received the B.S. and M.S. degrees in mechanical and aerospace engineering from Tokai University, Hiratsuka, Japan, in 2015 and 2017, respectively, and the Ph.D. degree in aerospace engineering from Tohoku University, Sendai, Japan, in 2020.

From 2018 to 2020, he was a Research Fellow of the Japan Society for the Promotion of Science (JSPS) at Tohoku University. He is currently a Project Assistant Professor at Tohoku University.

Keigo Yamada received the B.S. degree in physics from Tohoku University, Sendai, Japan, in 2019, where he is currently pursuing the Ph.D. degree with the Department of Aerospace Engineering.

He is currently a Research Fellow of the Japan Society for the Promotion of Science (JSPS) at Tohoku University.

Taku Nonomura received the B.S. degree in mechanical and aerospace engineering from Nagoya University, Nagoya, Japan, in 2003, and the Ph.D. degree in aerospace engineering from the University of Tokyo, Tokyo, Japan, in 2008.

He is currently an Associate Professor with the Department of Aerospace Engineering at Tohoku University, Sendai, Japan.

Kazuki Sakaki received the B.S. and Ph.D. degrees in aerospace engineering from the University of Tokyo, Tokyo, Japan, in 2012 and 2017, respectively.

He is currently a Researcher at the Japan Aerospace Exploration Agency (JAXA), Tsukuba, Japan.

Yoshio Nunome received the B.S. degree in mechanical and aerospace engineering and the Ph.D. degree in aerospace engineering from Tohoku University, Sendai, Japan, in 1999 and 2004, respectively.

He is currently an Associate Senior Researcher with the Research and Development Directorate, Japan Aerospace Exploration Agency, Kakuda, Japan.